Monthly Notices
of the
ROYAL ASTRONOMICAL SOCIETY

MNRAS **468,** 4151–4169 (2017)
Advance Access publication 2017 March 16

doi:10.1093/mnras/stx647

The metal-rich abundance pattern – spectroscopic properties and abundances for 107 main-sequence stars

O. M. Ivanyuk,[1]★ J. S. Jenkins,[2] Ya. V. Pavlenko,[1,3] H. R. A. Jones[3] and D. J. Pinfield[3]

[1]*Main Astronomical Observatory, National Academy of Sciences of Ukraine, Holosiyiv Wood, UA-03680 Kyiv, Ukraine*
[2]*Departamento de Astronomía, Universidad de Chile, Camino el Observatorio 1515, Las Condes, Santiago, 7591245, Chile*
[3]*Centre for Astrophysics Research, University of Hertfordshire, College Lane, Hatfield, Hertfordshire AL10 9AB, UK*

Accepted 2017 March 14. Received 2017 March 14; in original form 2015 November 3

ABSTRACT

We report results from the high-resolution spectral analysis of the 107 metal-rich (mostly [Fe/H] $\geq$ 7.67 dex) target stars from the Calan–Hertfordshire Extrasolar Planet Search programme observed with HARPS. Using our procedure of finding the best fit to the absorption line profiles in the observed spectra, we measure the abundances of Na, Mg, Al, Si, Ca, Ti, Cr, Mn, Fe, Ni, Cu and Zn, and then compare them with known results from different authors. Most of our abundances agree with these works at the level of $\pm$0.05 dex or better for the stars we have in common. However, we do find systematic differences that make direct inferences difficult. Our analysis suggests that the selection of line lists and atomic line data along with the adopted continuum level influence these differences the most. At the same time, we confirm the positive trends of abundances versus metallicity for Na, Mn, Ni and, to a lesser degree, Al. A slight negative trend is observed for Ca, whereas Si and Cr tend to follow iron. Our analysis allows us to determine the positively skewed normal distribution of projected rotational velocities with a maximum peaking at 3 km s^{-1}. Finally, we obtained a Gaussian distribution of microturbulent velocities that has a maximum at 1.2 km s^{-1} and a full width at half-maximum $\Delta v_{1/2} = 0.35$ km s^{-1}, indicating that metal-rich dwarfs and subgiants in our sample have a very restricted range in microturbulent velocity.

Key words: stars: abundances – stars: atmospheres – stars: fundamental parameters – stars: late-type – stars: rotation – stars: solar-type.

1 INTRODUCTION

Understanding the chemical make-up of stars like the Sun is fundamental to our understanding of star formation and stellar evolution. Edvardsson et al. (1993) undertook a classical study of the chemical evolution of the Galactic disc, deriving abundances for a sample of 189 nearby field F and G dwarfs. They found a number of interesting relationships in the data, for example, the strongest age-dependent abundance comes from Ba, which they attribute to the efficient s-element synthesis in low-mass AGB stars that enrich the interstellar medium long after star formation. They confirmed that metal-poor stars ([Fe/H] < -0.4 dex) are relatively overabundant in α-elements. Since the [α/Fe] for these stars shows a gradient that decreases with increasing Galactocentric distance of the orbits, they show that star formation was probably more vigorous and started first in the inner parts of the Galactic disc.

Since this work, various other samples have been studied, a number of which were performed by the exoplanet community (e.g. Valenti & Fischer 2005; Bond et al. 2008; Neves et al. 2009). These works have concentrated on studying the abundance distributions of exoplanet host stars compared with non-exoplanet hosts, and a number of interesting trends have been found. Along with the well-established dependence of giant planet detection probability on host star metallicity (Gonzalez 1997; Santos et al. 2008), these abundance analyses indicate that various other atomic abundances are likely enhanced in exoplanet hosts compared to non-exoplanet hosts (e.g. Si and Ni), at least for the gas giant population. These overabundances are explained in the framework of the core accretion scenario of planet formation (Livio & Pringle 2003; Ida & Lin 2008) where the more the disc material present, the higher the probability of planet formation.

In general, the relative yields of different elements in the atmospheres of stars change with time, due to the processes of nucleosynthesis in the Galaxy. These processes are still poorly known, yet performing high-quality analyses of homogeneous stellar samples can shed light on the fine underlying processes that are occurring, following the formation of planetary systems.

In recent years, a series of large-scale abundance analyses have been published (Valenti & Fischer 2005; Luck & Heiter 2006; Jenkins et al. 2008; Adibekyan et al. 2012; Bensby et al. 2014; Brewer et al. 2016), mainly driven by the availability of high-resolution

★ E-mail: oi@mao.kiev.ua

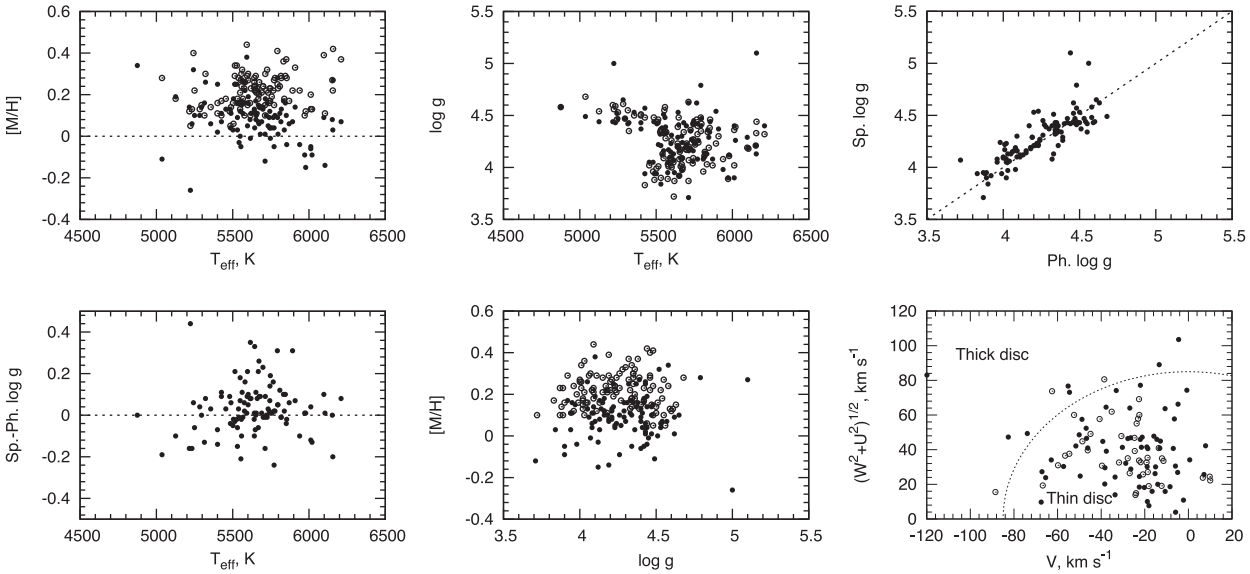

Figure 1. The general properties of the sample. The HARPS data, based on our spectroscopic $\log g$ values, are shown with filled circles. Mean error bars of our $T_{\rm eff}$, $\log g$ and [Fe/H] determinations are $\pm$50 K, $\pm$0.2 dex and $\pm$0.1 dex, respectively. The FEROS data, based on the photometric determinations of the $\log g$ parameter (Jenkins et al. 2008), are shown with open circles. Bottom right-hand panel: The Toomre diagram for 67 stars in the sample is shown, using the data taken from Murgas et al. (2013) (filled circles), and for the remaining 40 stars from Jenkins et al. (2011) (empty circles). The boundary between the thin and thick discs of the Galaxy is defined by following Fuhrmann (2004).

spectral data from observational campaigns that are dedicated to searching for planets and the proliferation of software that allows us to automatically process the spectra of hundreds of stars in an automatic, or semi-automatic, manner.

The analysis we provide here is used to determine the chemical abundances in the atmospheres of metal-rich stars, along with their relative behaviour versus iron. It is worth noting that our sample is one of the generally homogeneous samples (e.g. Adibekyan et al. 2012) in comparison to similar studies, which cover up to a thousand stars, but obtained using different instruments with different resolutions and pipeline reduction techniques (e.g. Bensby et al. 2014). On the other hand, some homogeneous studies cover rather a smaller number of stars (e.g. Feltzing & Gustafsson 1998; Bruntt et al. 2002; Gillon & Magain 2006) or with lower resolution (e.g. Luck & Heiter 2006). In this work, we combined both a large enough sample and high resolution to provide us with a good statistical sample to investigate.

The layout of the manuscript is as follows: In Section 2, we discuss the observational data; in Section 3, we describe the method used to derive the abundances, $T_{\rm eff}$ and $\log g$, our selection criteria of the examined lines and the influence of the microturbulence and rotation. Section 4 contains the description of our results, and in Section 5, we compare these results to the previously published works. Finally, in Section 6, we discuss the implication of our results in the field, and summarize our findings in Section 7.

2 OBSERVATIONS

The Calan–Hertfordshire Extrasolar Planet Search (CHEPS) programme (Jenkins et al. 2009) is monitoring a sample of the metal-rich stars in the Southern hemisphere, to improve the statistics for planets orbiting such stars, along with searching for short-period planets that have a high probability to transit their host star. All stars in the sample were initially selected from the *Hipparcos* catalogue (Perryman et al. 1997) to have V-band magnitudes in the range of 7.5–9.5. This range ensures that the sample is not overlapping with existing planet search programmes, since most solar-like stars with magnitudes below 7.5 are already being examined as part of other planet search programmes, and the upper limit is set to ensure that the stars are bright enough to allow the best follow-up to search for secondary eclipses and transmission spectroscopy, essentially bridging the gap between the long-term precision radial velocity programmes and the fainter samples that photometric transit surveys are generally biased towards.

More specifically, the CHEPS sample primarily contains objects that were drawn from a larger southern sample observed using the European Southern Observatory-FEROS spectrograph (see Jenkins et al. 2008, 2011). The secondary selection of these targets was focused on the inactive ($\log R'_{\rm HK} \leq -4.5$ dex) and metal-rich ([Fe/H] ≥ 0.1 dex) subset of this sample (Jenkins et al. 2008) to ensure the most radial velocity stable targets, and to make use of the known increase in the fraction of planet-host stars with increasing metallicity. We note that recent work has shown that the fraction of metal-rich stars hosting low-mass planets may not follow the metallicity trend observed in the gas giant population (Buchhave et al. 2012; Jenkins et al. 2013a).

Our subset of targets has been followed up using HARPS at La Silla in Chile. In our analysis, we use high signal-to-noise ratio (S/N) (>100) and high-resolution spectra ($R \sim 120\,000$) of predominantly single stars from the CHEPS sample that have been well characterized photometrically based on *Hipparcos* data (Jenkins et al. 2008, 2009, 2011).

The general properties of the sample are shown in Fig. 1. Jenkins et al. (2008) carried out the photometric determinations of the surface gravity parameter for our stars (shown with open circles), and we compare these values to our spectroscopically measured $\log g$ (filled circles). We work within a narrow $T_{\rm eff}$ range between 5200 and 6200 K, with the majority of our stars being metal rich and on the main sequence ($\log g > 4.1$), although a few are slightly metal deficient ([Fe/H] > -0.2). Most of the stars in our sample belong

to the thin disc Galactic population; see the Toomre diagram at the bottom right-hand side of Fig. 1.

3 SYNTHETIC SPECTRA ANALYSIS

3.1 Abundances and surface gravities

We used a modified numerical scheme developed by Pavlenko (2002, 2017); Pavlenko et al. (2012) that allows us to determine the atomic abundances, rotational velocities, microturbulences and surface gravities in the stellar atmospheres from high-resolution and high-S/N spectra, all in the framework of an iterative approach, i.e. at each new step, the model atmospheres and synthetic spectra were recomputed for the metallicities and gravities derived before in our procedure, and for the fixed effective temperatures that were set photometrically.

The method is based on the minimization of differences in the profiles of computed and observed lines. We used the two independent procedures for the final model parameters. First, we required no dependence of the Fe I abundance on the line strengths to obtain $V_{\rm m}$. Secondly, we required the agreement between the abundances of Fe I and Fe II obtained for the previously found $V_{\rm m}$ to determine $\log g$.

For our starting point, we used the photometrically determined metallicities and $\log g$ (see Jenkins et al. 2008), then we ran a few iterations to determine [Fe I/H], $V_{\rm m}$, [Fe II/H] and $\log g$. The final step was the determination of abundances and $V_r \sin i$ for the model atmosphere parameters found in the procedure before.

All synthetic spectra were computed by the WITA6 program (Pavlenko 1997) using 1D local thermodynamic equilibrium (LTE) model atmospheres computed with the SAM12 code (Pavlenko 2003) combined with the minimization routine ABEL8 (Pavlenko et al. 2012; Pavlenko 2017). The lines to be fitted in the stellar spectra were compiled using the solar spectrum by Kurucz et al. (1984) and atomic line data from VALD-2 and VALD-3 (Kupka et al. 1999; Ryabchikova et al. 2015).

In our analysis, we made a few basic assumptions: The level of activity is low in these atmospheres; in other words, the continuum in the optical range forms in the photosphere of the star. Both the microturbulent and macroturbulent velocity fields are similar to the solar case. For simplicity, we adopt that $V_{\rm macro}$ and $V_{\rm m}$ do not change with the depth in these atmospheres. The convection zone is similar to the solar convection zone, even in the case of super-metal-rich stars. The minimum of the atmospheric temperature is located above the line formation region. Spots on the surface of these stars are not sufficiently numerous to contribute to the formation of absorption lines or continuum, in terms of the emitted fluxes. Naturally, if any of these assumptions is not valid for the physical state of the studied stars, we will obtain a spread of abundances and other determined parameters, even in the case of ideally determined $T_{\rm eff}$ and $\log g$.

3.2 Effective temperatures

The effective temperatures were estimated using the photometric methods (see Jenkins et al. 2008), exploiting the existing large photometric data bases, along with the latest relationships between stellar broad-band colours and their photospheric effective temperatures. Namely, we used the Johnson V-band photometry that was taken from the *Hipparcos* data base (Perryman et al. 1997) as our optical anchor point, and combined this with near-infrared photometry from the 2MASS data base (Struskie et al. 2006), in particular, the $K_{\rm s}$-band magnitude that gives a sufficiently large wavelength baseline to sample the shape of the spectral energy distribution. We then used the relationships provided in Casagrande et al. (2010) to calculate accurate effective temperatures and place the stars on a Hertzsprung–Russell diagram to calculate the photometric $\log g$ values using the Y2 evolutionary models (Demarque et al. 2004).

We choose to use these photometric $T_{\rm eff}$ for the computations, rather than update them spectroscopically. We believe that this constrains uncertainties that may arise from the quality of fits to the spectra and atomic line data, and these may also affect the results of our determination of abundances, microturbulent velocities and surface gravities.

3.3 Line lists

We provide our analysis for the pre-selected list of spectral lines extracted from VALD-2 and VALD-3 (Piskunov et al. 1995; Kupka et al. 1999; Ryabchikova et al. 2015). To create the list of 'reliable' lines for each element, we computed the solar synthetic spectra and convolved them to get the effective resolving power of $R \sim 70\,000$, which is the effective resolution due to macroturbulent velocity field in the solar atmosphere.

The theoretical spectra were fitted to the selected observed lines using the minimization routine ABEL8. At this stage, we excluded severely blended lines, too weak lines with residual fluxes lower than 20 per cent and strong lines with $r_{\rm nu} > 0.7$ to minimize the distortion of the results due to noise and possible non-LTE effects in the cores of the strong lines (Mashonkina et al. 2011).

We computed our synthetic spectra using the damping constants provided by VALD (Kupka et al. 1999). For the absorption lines without damping constants, we computed them using the Unsold formulae (Unsold 1955).

The fitting part of each line profile was adopted manually to reduce the uncertainties introduced by wing blending. In some cases, very close blends of the lines of the same element were fitted together, resulting in a single spectral range to fit multiple lines. The final list of fitting ranges for the neutral and ionized atoms available on CDS.

3.4 Microturbulent velocities

The microturbulent velocity is an important parameter in 1D line-profile-fitting techniques as there is an evident trend with abundances that causes uncertainties in their measurements. The dependence of Fe I and Fe II abundances on microturbulent velocity for HD 102196 is shown in Fig. 2. Here, Fe I and Fe II abundances differ by up to ± 0.1 dex at $V_{\rm m} = 1.0$ km s^{-1} but are the same at 1.4 km s^{-1}.

We carried out a set of synthetic spectra fits to Fe I and Fe II lines independently, using the grid of adopted microturbulent velocities in the range from 0.0 to 2.6 km s^{-1}, with a step of 0.2 km s^{-1}. In fact, we followed the procedure of Pavlenko et al. (2012), but here we investigated the dependence of $D_a = \partial a / \partial r_{v_0}$, where a and r_{v_0} are the abundance and the central intensity of the corresponding iron absorption line computed for the grid of $V_{\rm m}$, and the D_a is known to show the dependence on $V_{\rm m}$. Therefore, we determine our $V_{\rm m}$ at $D_a = 0$.

Our procedure is based on fitting to the line profiles, excluding the shallow parts of the wings, which could be more affected with blending by the weak lines of other elements. Furthermore, the wings of lines are more affected by the pressure broadening than the microturbulent velocities. Accounting both these factors should improve the determination of $V_{\rm m}$ (see Fig. 5).

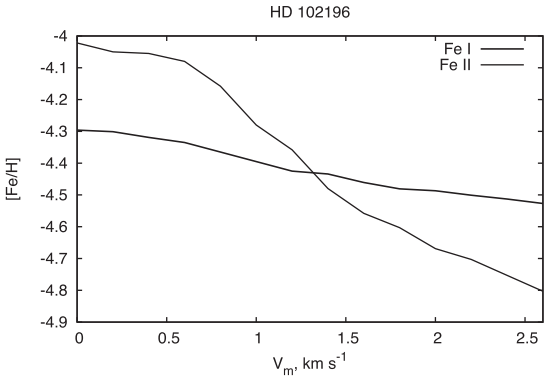

Figure 2. The dependence of Fe I and Fe II abundances on the microturbulent velocity obtained from the fits of our synthetic spectra for the model atmosphere $T_{\rm eff}$/log g= 6012/3.90 to the observed HD 102196 spectrum.

3.5 Rotational velocities

The profiles of absorption lines in the stellar spectra are affected by the rotation of a star, depending on the magnitude of rotation. The rotational profile, in our case, determined by the formula of Gray (1976), is of a different shape compared to the instrumental broadening and macroturbulence. In our analysis, each line of the synthetic spectra was convolved with a profile of a different V_r sin i, and was fitted to the observed spectra until the best result was found. Despite we used only Fe I lines for the determination of V_r sin i, the procedure was also applied for every other line of all our elements to get a better fit to the observed line profiles.

4 RESULTS

4.1 Rotational velocities

We found that the majority of our stars are slow rotators, with V_r sin $i < 4$ km s^{-1}(Fig. 3). Likely, a few stars with larger rotational velocity present the cases where sin $i \sim 1$, rather than large V_r itself, since these stars are of lower activities, with only a few fast-rotating active stars left over.

On the other hand, V_r sin i correlates with log g, older stars rotate slower, in agreement with the theory, and vice versa, which is in line with their ages given by the preliminary CHEPS selection. We can see an uprising trend of V_r sin i for the stars of lower log g, which represent a younger population.

For the elements other than Fe I, V_r sin i was used rather as the adjusting parameter. Nevertheless, it agreed for the properly fitted lines of different elements within an uncertainty of less than 1 km s^{-1}. We can claim a clear measurement for the values of V_r sin $i > 2$ km s^{-1}. Uniform results for the iron lines give credibility to our results.

4.2 Solar abundances

We carried out a differential analysis with respect to the Sun as a star, since our line lists were selected based on a comparison of the synthetic spectra to the observed solar spectrum by Kurucz et al. (1984). This allowed us to minimize possible blending effects, at least in the solar case.

We performed a quantitative analysis of the solar abundances to verify our procedure. Computations were done for the initial model atmosphere with $T_{\rm eff}$/log g/[Fe/H] = 5777/4.44/−4.40, computed using SAM12 (Pavlenko 2003).

For the iron ions, we obtained N(Fe I) = −4.42 ± 0.03 and N(Fe II) = −4.46 ± 0.02 dex, which again highlights the known problem of the measured difference between Fe I and Fe II abundances obtained in the framework of the classical approach (see Holweger et al. 1990; Shchukina & Trujillo 2015; Shchukina, Sukhorukov & Trujillo 2016). The abundances for the other elements (see the first column of Table 2) are in agreement with those in the literature (e.g. Anders & Grevesse 1989; Asplund et al. 2009).

We also determined the microturbulence and projected rotational velocity for the Sun as a star, measuring $V_{\rm m} = 1.0 \pm 0.2$ km s^{-1} and V_r sin $i = 1.69 \pm 0.09$ km s^{-1}, which also agree with known results. The solar abundances determined for the different atomic line data and line lists are discussed in Section 5.

4.3 Stellar abundances

The complete table of abundances is available on CDS. In our analysis, we used the parameter X_f to describe the average slope of the distribution of abundances for a given element relative to iron. We computed X_f using a standard least-squares approach to approximate the dependence of [X/Fe] on [Fe/H] by a linear function. By definition, X_f characterizes, to first order, the relative changes of the yield of elements with respect to the iron.

In order to make a useful comparison with other works, we needed to translate on to a common scale. We found that the easiest way to achieve this was to adopt the scale of Anders & Grevesse (1989) rather than in terms of the solar abundances determined by our procedure. In some papers, abundances are provided in relation to derived solar scales in order to compensate for the differences in procedures (e.g. Bensby et al. 2014; Brewer et al. 2016). Other authors adopt Anders & Grevesse (1989) or its later derivatives (e.g. Valenti & Fischer 2005; Adibekyan et al. 2012), though they did not consider their derived solar abundances. In order to compare the different samples studied by different authors, we converted

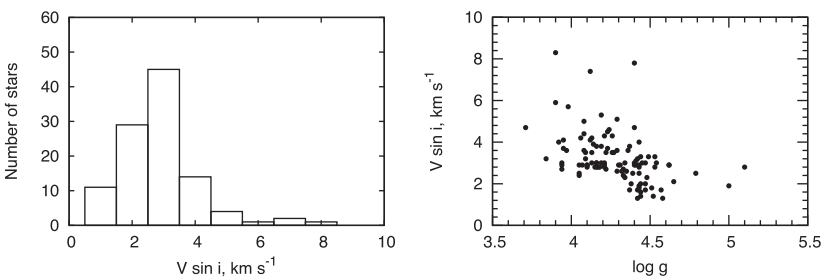

Figure 3. Left-hand panel: The histogram shows the distribution of rotational velocities V_r sin i for the stars in our sample. Right-hand panel: the dependence of V_r sin i on log g.

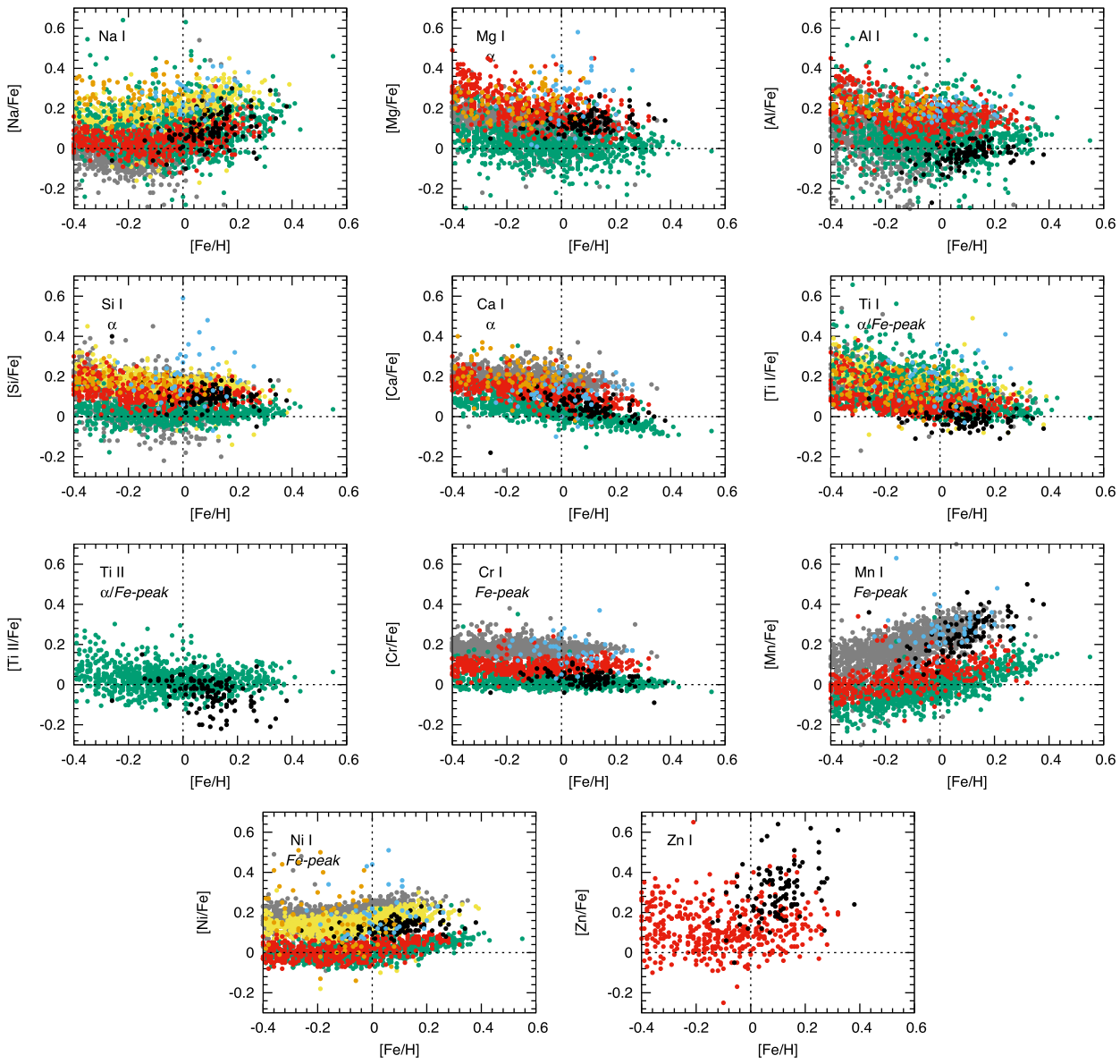

Figure 4. The comparison of [X/Fe] versus [Fe/H] in the samples by Edvardsson et al. (1993) – shown with orange, Feltzing & Gustafsson (1998) – with blue, Valenti & Fischer (2005) – with yellow, Adibekyan et al. (2012) – with green, Bensby et al. (2014) (Battistini & Bensby 2015, in case of Mn) – with red, Brewer et al. (2016) – with grey, and this work – with the black circles. The reference solar abundances for each work are converted to the scale of Anders & Grevesse (1989).

abundances for the various comparison samples into the scale of Anders & Grevesse (1989) (Fig. 4). This also allowed us to assess the general accuracy level of stellar abundance determinations from the combined spread of abundances.

In Fig. A3, we show the dependence of abundances relative to iron with their corresponding error bars. These uncertainties depend on the number of lines for each element, quality of fit, the scatter of abundances determined from the fits to different lines, the local continuum level and the atomic line data taken from VALD. The uncertainties for [Fe/H] are not plotted to make the plots easier to read. The average [Fe/H] uncertainty is ±0.02 dex.

Below we discuss the specific results for the selected elements:

(i) Fe, $Z = 26$. Differences up to 0.1 dex between Fe I and Fe II abundances are due to the iterative nature of our computations. Previously determined abundances can change after the adoption of the refined model atmosphere. In other words, it reflects the limit of accuracy implied by the model atmosphere, atomic line data and line list.

(ii) Na, $Z = 11$. The distribution of the Na abundance versus iron is shown in Fig. 4. The computed X_f for the metal-rich stars in our sample and those of Adibekyan et al. (2012) and Bensby et al. (2014) show a well-defined positive slope (Table A1). The abundance distribution of Na is shifted towards larger abundances by 0.1–0.2 dex compared to Fe. The general trend is similar to those obtained in all comparison works with higher abundances towards higher metallicities (Fig. 4).

(iii) Mg, $Z = 12$. Only up to seven lines of Mg I were used in the analysis. We found a similar result to that of sodium, with a notable overabundance for our sample, and a mean abundance of

[Mg/Fe] = 0.13 ± 0.05 dex. The shift is larger than the formal accuracy of our abundance determination procedure, but may depend on the adopted continuum level and line list. We note that $X_f > 0$ for the stars in our sample. However, it can be seen in Fig. 4 that this could be due to border effects, as this trend is rather marginal. Bensby et al. (2014) show the same order of overabundance, but also a certain downward trend with metallicity, and for the sample of Adibekyan et al. (2012), we see that their Mg distribution is in agreement with [Fe/H]. At the same time, Brewer et al. (2016) show the results similar to ours.

(iv) Al, $Z = 13$. In our work, aluminium shows a definite positive slope. To some degree, our findings are similar to those of Adibekyan et al. (2012) and Brewer et al. (2016), but different from Edvardsson et al. (1993); Feltzing & Gustafsson (1998) and Bensby et al. (2014), who show no definite dependence on metallicity, and higher mean [Al/Fe] for their samples.

(v) Si, $Z = 14$. The results for silicon agree well with most of the studies in comparison, showing the average [Si/Fe] overabundance to be of the order of 0.1 dex and no noticeable trend with metallicity. On the other hand, Adibekyan et al. (2012) show no excess of silicon. It is interesting to note that for the same lines in the spectra, our results for VALD-2 show 0.1 dex lower abundances than for VALD-3, highlighting the importance of reliable atomic line data.

(vi) Ca, $Z = 20$. Calcium is another element for which we see a high level of agreement between the different authors (Edvardsson et al. 1993; Feltzing & Gustafsson 1998; Adibekyan et al. 2012; Bensby et al. 2014; Brewer et al. 2016). In all these works, there is a clear negative trend with metallicity (Table A1). On the whole, [Ca/Fe] > 0, but in the super-metal-rich domain, we note calcium deficiency. However, various mean abundances in different works (see Fig. 4) reflect that this deficiency is within the accuracy limit of the modern methods of abundance determination.

(vii) Ti, $Z = 22$. In our sample, Ti I follows the iron abundance and shows no dependence on metallicity. On the other hand, all comparison works show a larger spread of stars towards higher [Ti/Fe] abundances and a weak negative trend. At the same time, Adibekyan et al. (2012) show no metallicity dependence for Ti II. For our stars, the Ti II lines show a large scatter, which makes it difficult to come to any firm conclusions in regards to the metallicity trends. Similar to Si I and Fe II, the lines of ionized titanium give rise to a 0.1 dex higher abundance when the line parameters are taken from VALD-3.

(viii) Cr, $Z = 24$. Chromium is one of the few elements with reliable results that show no significant scatter between the different lines and stars in our sample. We can observe a very weak negative trend with iron. The same results are shown by Adibekyan et al. (2012). Bensby et al. (2014) and Brewer et al. (2016) show higher abundances for their stars and a weak positive trend, which could be an indication of the sample bias effect. Once again, the same chromium lines give different abundances using the different versions of VALD, but unlike Si I, Ti II and Fe II, we see a 0.05 dex lower mean abundance for the VALD-3 data.

(ix) Mn, $Z = 25$. Manganese abundances show a clear positive gradient with metallicity, much like Zn, though with a larger scatter, despite the relatively large number of lines used in the analysis. Manganese exhibits a higher abundance than iron, on average, by 0.3 dex. A positive trend was also found in all comparison works. As for most of the other elements, the abundance measured by Bensby et al. (2014) is slightly higher than that of Adibekyan et al. (2012). Feltzing & Gustafsson (1998) and Brewer et al. (2016) show the results similar to ours (Fig. 4).

(x) Ni, $Z = 28$. [Ni/Fe] also shows an upward trend with iron of the same order in all the samples in comparison. All the authors show different average overabundances for Ni: up to 0.05 dex for Adibekyan et al. (2012) and Bensby et al. (2014), 0.1 dex for Feltzing & Gustafsson (1998) and our work, and 0.15 dex for Valenti & Fischer (2005) and Brewer et al. (2016).

(xi) Cu, $Z = 29$. The distribution of Cu with [Fe/H] exhibits a large scatter (Fig. A3), mainly affected by the quality of the line list and number of lines. Formally speaking, within the range of metallicities [Fe/H] = −0.1 to +0.2, there are two groups of stars, with mean [Cu/Fe] abundances of ∼+0.1 and −0.05 dex, respectively, however, with uncertainties at the level of ±0.4 dex. The lower average abundances and defined positive trend were found by da Silva, Milone de & Rocha-Pinto (2015). The same trend could be observed for the ∼0.0 dex group of stars in our sample.

(xii) Zn, $Z = 30$. For Zn, we found the same significant differences in the abundance distribution with iron as found for manganese. Unfortunately, we used only one line of Zn in our analysis, so the visible slope of [Zn/Fe] versus [Fe/H] should be considered as a preliminary result at this point. More work should be done to confirm this result using a wider set of Zn atomic lines. A large scatter and similar abundance are also shown by Bensby et al. (2014) and Nissen (2015).

Our analysis shows that the different atomic line data can have a strong impact on the average abundances measured for similar samples of stars (e.g. see silicon in this work). On the other hand, observed trends change rather marginally. Comparisons to our work and those in the literature highlight similar tendencies for Na, Si, Ca, Cr, Mn and Ni; for the elements with a small spread like Si, Ca, Cr and Ni, we see various average abundances between the different samples, and similar trends with iron in all comparison works. And for Mg, Al and Ti, we see weak trends with iron in all comparison works due to a large spread of abundances.

4.4 The dependences on $T_{\rm eff}$ and $\log g$

In the framework of our work, we investigated the dependence of our abundance results on the effective temperature and surface gravity. The results of these tests are shown in Figs A1 and A2. We see the evidence for a weak trend of abundances versus $T_{\rm eff}$ in Fig. A1. These rather indistinct trends may be explained by uncertainties in the choice of the photometric $T_{\rm eff}$ of the metal-rich stars of earlier spectral classes, as well as limitations of the current model atmospheres and atomic line data. In each case, we obtained the trends of abundances versus $T_{\rm eff}$ for the elements with rather low ionization potentials, i.e. Mg, Al and Si, with the Pearson product–moment correlation $\rho(T_{\rm eff}) \sim 0.4$–$0.5$ (Table A1). We observe the same for Mn and Zn. However, because our data do not show a sufficient level of homoscedasticity, it is hard to make definitive conclusions in this regard.

We note the non-linear behaviour of the [X/H] versus $T_{\rm eff}$ dependence for practically all our elements in the stars with $T_{\rm eff}$ close to 6000 K. This apparent 'phantom' gap is poorly constrained due to a low number of stars in this temperature range.

What is more important is that we do not see any evident trends of the abundances versus the adopted surface gravities (Table A1). In some sense, this provides us with the evidence that our adopted procedure performs in the way we previously envisaged it would.

However, the sensitivity of the spectroscopic $T_{\rm eff}$ and $\log g$ to the quality of fits and line data (discussed in Section 5) emphasizes the importance of at least one independent variable.

Table 1. The procedures used for the abundance analysis in some recent works. Note that the papers by Neves et al. (2009), Sousa et al. (2011) and Adibekyan et al. (2012) belong to the same series of works. Here, R labels the resolution of the observed spectra, EW denotes equivalent width measurements, SS is synthetic spectra fitting and X_i stands for the abundances.

Paper	Targets	Procedure	Output
Valenti & Fischer (2005)	1040 HIRES, UCLES, Hamilton, R 70K	SS, ATLAS9, SME	X_i, $T_{\rm eff}$, $\log g$, $V_r \sin i$
Jenkins et al. (2008)	353 FEROS, R 46K	SS, SAM12, WITA6	X_i, $V_r \sin i$
Neves et al. (2009)	451 HARPS, R 120K	EW, MOOG, ARES	X_i, $T_{\rm eff}$, $\log g$, $V_{\rm m}$
Sousa et al. (2011)	582 HARPS, R 120K	EW, MOOG, ARES	X_i, $T_{\rm eff}$, $\log g$, $V_{\rm m}$
Adibekyan et al. (2012)	1111 HARPS, R 120K	EW, MOOG, ARES	X_i, $T_{\rm eff}$, $\log g$, $V_{\rm m}$
Bensby et al. (2014)	60 FEROS, R 48K 5 HARPS, R 120K 27 UVES, R 110K 31 UVES, R 80K 52 SOFIN, R 80K 6 FIES, R 67K 374 MIKE, R 65K 49 MIKE, R 42K 79 MIKE, R 55K	EW, MARCS, IRAF	X_i, $T_{\rm eff}$, $\log g$, $V_{\rm m}$
da Silva et al. (2015)	309 ELODIE, R 42K	EW, MOOG, ARES	X_i, $T_{\rm eff}$, $\log g$, $V_{\rm m}$
Brewer et al. (2016)	1626 HIRES, R 70K	SS, ATLAS9, SME	X_i, $T_{\rm eff}$, $\log g$, $V_r \sin i$
This work	107 HARPS, R 120K	SS, SAM12, ABEL8	X_i, $\log g$, $V_r \sin i$, $V_{\rm m}$

5 COMPARISON TO OTHER AUTHORS

There have been a number of extensive works to determine abundances of main–sequence dwarfs. They follow similar approaches to the analysis of the observed high-resolution stellar spectra: LTE, 1D model atmospheres. We tabulate these in Table 1.

To compare our results to other authors, we note that our sample primarily consists of metal-rich stars; the samples of some other authors consist of a larger total number of targets, and they maintain a broader metallicity range. Most of our objects are single stars, where our spectroscopic data have been observed solely using HARPS, using a photometric pre-selection, and thus our sample is homogeneous.

Though most of comparison works were done using the equivalent width analysis, we used the synthetic profile fitting. In comparison to Valenti & Fischer (2005) and Brewer et al. (2016), who utilized synthetic spectra fitting for the broad spectral ranges and fixed microturbulent velocity, we adopted line-by-line fitting and microturbulence as a free parameter in addition to the other differences.

As noted in Section 4.3, some authors used their own solar abundances for the [X/Fe] distribution analysis, whereas we used the Anders & Grevesse (1989) abundances in our study. In our work, we separated the relative and absolute solar scales. The first case is defined by the reference solar abundances to which the absolute values are translated. And the second case is dependent on the adopted line lists and *gf*-values. We identify the latter as the differences in the atomic line data or line lists, but not in the adopted solar scales.

5.1 Microturbulent velocities

The microturbulent velocity is an important parameter that must be understood with as much precision as possible to properly determine the chemical abundances. We compare our distribution of $V_{\rm m}$ to those by the other authors across the metal-rich domain ([Fe/H] $\geq$ 7.67 dex) of their samples (Figs 5 and 6). $V_{\rm m}$ in the atmospheres of our stars lies in the range of 1.0–1.4 km s^{-1}, with the well-defined peak at 1.2 km s^{-1}. The peaks of the distributions in comparison are at 0.8–1.0 km s^{-1}.

In general, all distributions are of a similar shape. At the same time, our distribution of $V_{\rm m}$, determined from the fits to the observed line profiles, is narrower ($\sigma = 0.147$) than the similar distributions ($\sigma > 0.2$) obtained from the equivalent width analyses provided by the different authors independently on the number of stars used.

5.2 The common stars

We carried out a detailed comparison of our results to Bensby et al. (2014) and a few other authors (Fig. 7). These are the only works that have stars in common and references to the solar scales in use, which are essential for a direct abundance comparison.

In total, we found 26 stars from our sample that were previously analysed. The full list is given in Table A4. Note that the data in Table A4 are given 'as is' – with the [M/H] values provided in the solar scales adopted by the respective authors. Note the main differences between our procedures:

(i) The stars in common were observed using different spectrometers, and processed using different pipeline procedures.

(ii) We used different systems of the oscillator strengths *gf*, damping constants and the line lists.

(iii) In our analysis, we reproduced the absorption line profiles, and the other works reproduced the observed equivalent widths.

(iv) As mentioned above, the different types of analyses as well as the sample bias effects could lead to the different distributions of the microturbulent velocities (Fig. 5) and hence the abundances (Fig. 2).

This work as well as the comparison papers provided values that were measured relative to the Sun as a star. We do not expect large differences to be present here, and despite the various procedures and observed data, we find a good agreement between the different authors. Details of this analysis and observed differences are discussed in the following section.

A direct comparison of abundances for the common stars (Fig. 7) shows approximately the same values for Na, Mg, Si and Ca relative to iron in the different works. The agreement is within 0.02 dex.

For the Ti, Cr and Ni, we have slightly higher deviations of the order of 0.05 dex. For the first two elements, our abundances are

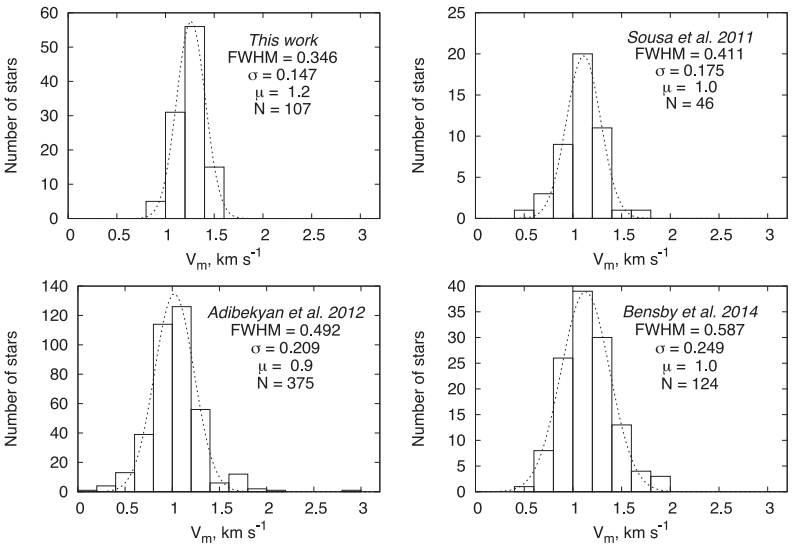

Figure 5. Distributions of microturbulent velocities for the metal-rich domain ([Fe/H] $\geq$ 0.0) in this work and from the results by Sousa et al. (2011), Adibekyan et al. (2012) and Bensby et al. (2014). Parameters μ and σ are the mean of the distribution and standard deviation, FHWM is the full width at half-maximum and N is the number of stars with [Fe/H] $\geq$ 0.0 dex in the comparison samples.

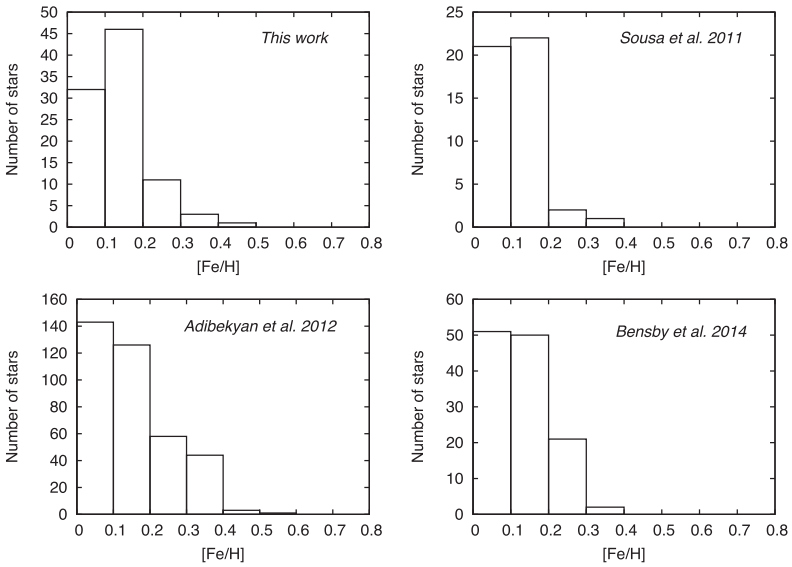

Figure 6. Distributions of metallicities in this work and from the results by Sousa et al. (2011), Adibekyan et al. (2012) and Bensby et al. (2014).

systematically lower, and Ni in our case is overabundant within the same range.

We found larger differences for the abundances of Al, Mn and Zn. This might be explained by differences in the line lists used; at least the distributions of stars in the different samples (Fig. 4) point to this conclusion. We got 0.1–0.2 dex higher abundances of Mn and Zn, and 0.1–0.2 dex lower for Al. However, our aluminium and manganese distributions agree with Adibekyan et al. (2012) and Feltzing & Gustafsson (1998), respectively, and our results agree with Brewer et al. (2016) for both these elements within the error bars.

5.3 Stability of the results

To verify the stability of our results, we re-determined fundamental parameters and abundances for the stars in common and the Sun using the effective temperatures, atomic line data and line lists by Bensby et al. (2014), and atomic line data from the second and third releases of VALD.

Bensby et al. (2014) analysed the spectra obtained using the MIKE spectrograph with an effective resolution of $R \sim 42\,000$–$65\,000$. By using their fundamental parameters and the line lists, we reduced the differences between our works to the different quality spectra, the different algorithms of $\log g$ and $V_{\rm m}$ determination, and the algorithms of abundance computations. We fitted our theoretical spectra to the observed line profiles; Bensby et al. (2014) carried out the equivalent width analysis. The results are summarized in Figs 8 and 9.

Our microturbulent velocities agree within ± 0.1 km s^{-1} for 8 stars out of 10, and for the remaining 2 stars within ± 0.2 km s^{-1}.

The differences in $\log g$ do not exceed 0.1 dex for most stars, and only two objects show a deviation up to 0.4 dex. The same two stars

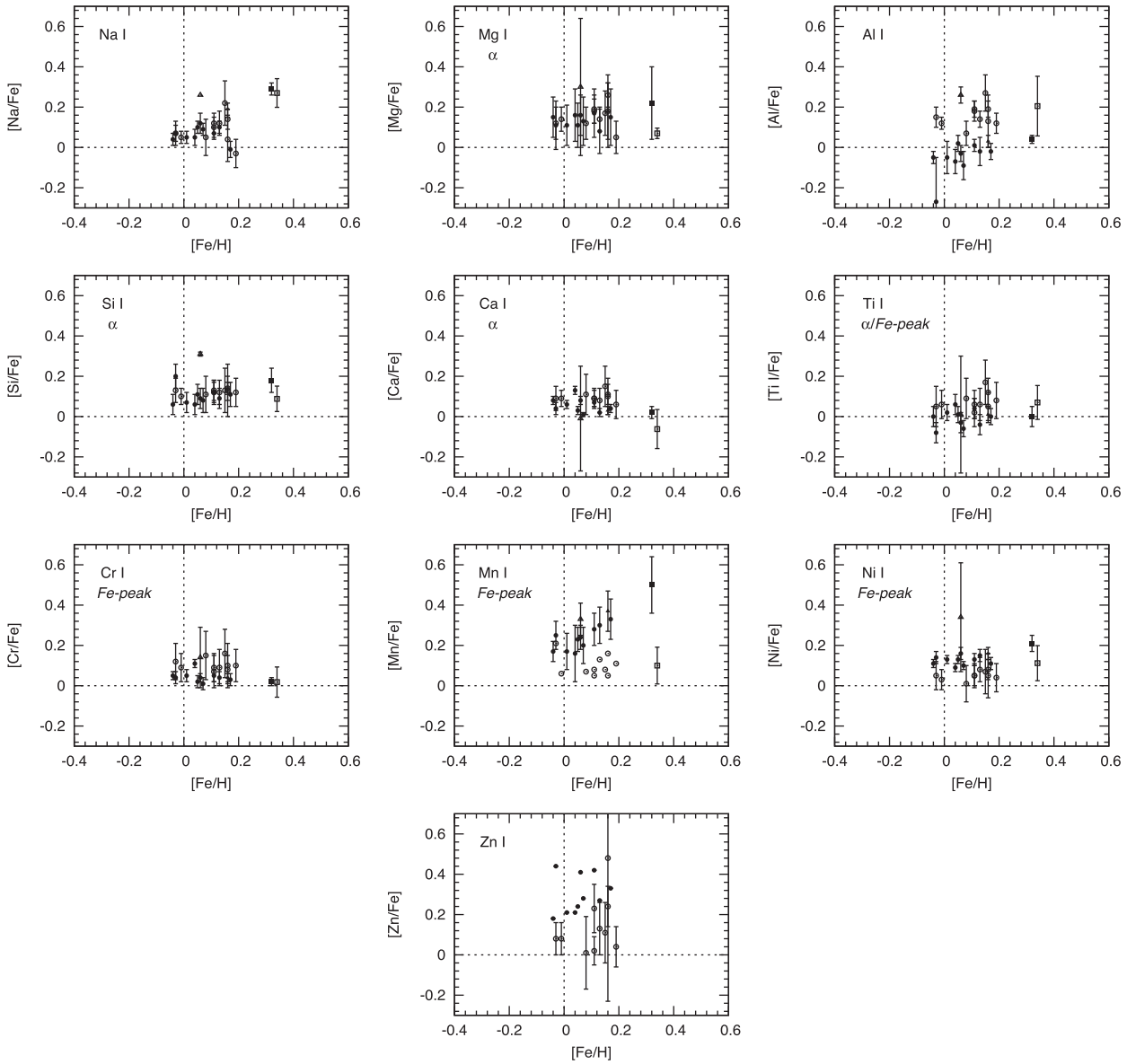

Figure 7. The dependences of [X/Fe] versus [Fe/H] for the common stars with Feltzing & Gustafsson (1998), Adibekyan et al. (2012) and Bensby et al. (2014) (Battistini & Bensby 2015, in the case of Mn) – shown with empty triangles, squares and circles, respectively. Our stars are drawn using the same figures, but filled. The reference solar abundances for each work are converted into the scale of Anders & Grevesse (1989).

also show an abundance difference up to 0.2 dex for the neutral iron in the worst case, but still within the error margin provided by Bensby et al. (2014) (Fig. 9).

As for the other elements, one of the reasons for differences was the limited number of lines that we were able to use. Indeed, due to the wavelength range of HARPS, we were able to use only a fraction of the line list provided by Bensby et al. (2014). We discuss the two other main factors further in the text.

The dependence on the different sets of atomic line data can be assessed using the example of the solar spectrum analysis. The results are summarized in Table 2. Note that in the cases of VALD-2 and VALD-3, we used the same line lists and fitting ranges that we used for our stars. The only difference was the atomic line data adopted in different versions of the data bases. In the case of Bensby et al. (2014), as mentioned above, we used only a fraction of their original line list.

VALD-2 and VALD-3 show the most notable difference of 0.2 dex for Si, which is also true for all the stars in our sample. Surface gravity is another notable issue that comes from the systematically lower Fe II abundances than those for Fe I for the initial solar model atmosphere.

For the case of Bensby et al. (2014), we also note the log g issue, which comes from the higher measured abundances for the Fe II lines and the notable differences of the order of ∼0.1–0.3 dex for Na, Mg, Al and Cr.

The main problem was that we could not well reproduce the solar equivalent widths obtained by Bensby et al. (2014) using their line list, oscillator strengths and model atmospheres.

We found two main reasons for these differences. First, the correction factor of the van der Waals broadening that was adopted by Bensby et al. (2014) was two times higher than in our case of using unmodified VALD damping constants (see Section 3.3). Once

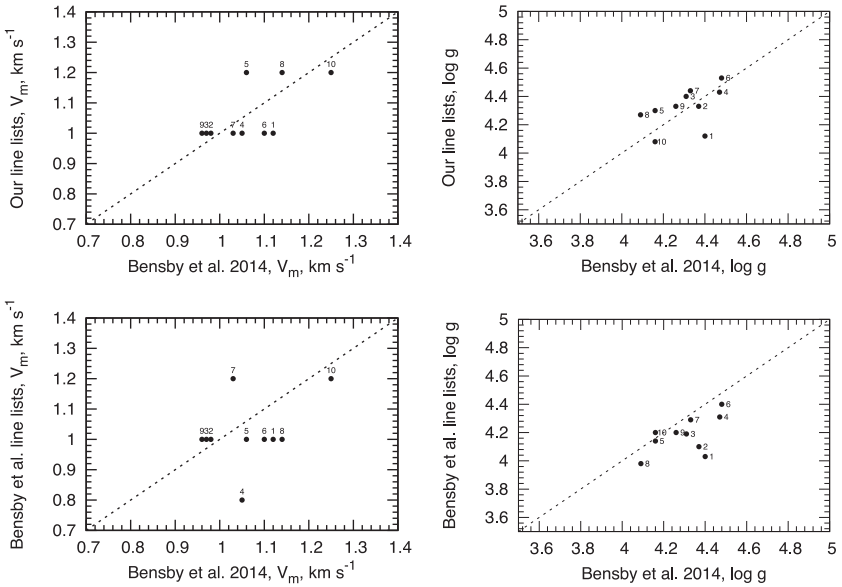

Figure 8. The comparison of microturbulent velocities and gravities for the common stars with Bensby et al. (2014), using our (top panel) and their line lists and effective temperatures (bottom panel). Here and forth, the data point numbers correspond to HD 150936, HD 165204, HD 170706, HD 185679, HD 186194, HD 190125, HD 194490, HD 218960, HD 220981 and HD 90520, respectively.

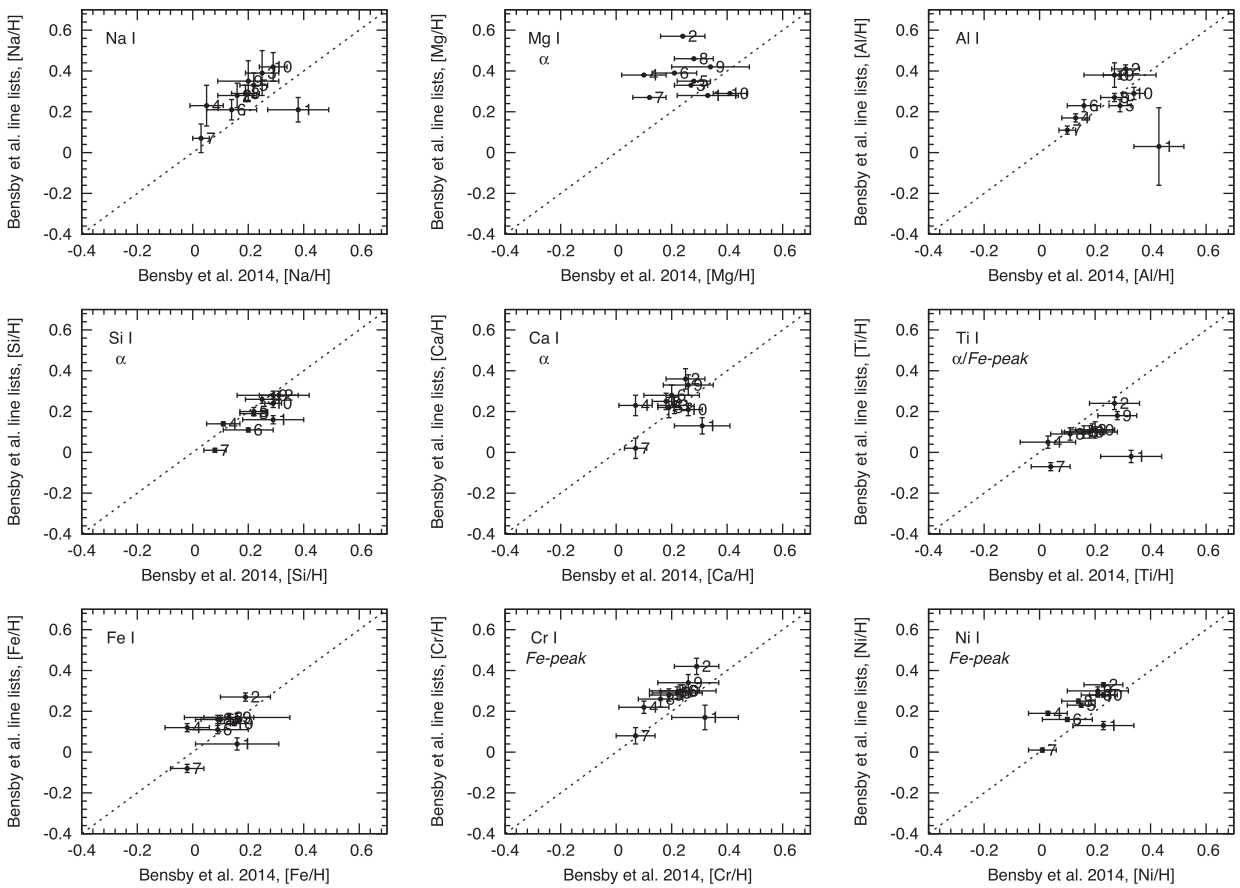

Figure 9. The comparison of abundances for the common stars with Bensby et al. (2014), using their line lists and effective temperatures.

we applied the correction, we were able to reproduce their equivalent widths. Secondly, the standard continuum levels in the solar spectrum by Kurucz et al. (1984) that we used in our work were different from those adopted by Bensby et al. (2014) for certain lines.

In Fig. 10, we show two of our fits to the solar spectrum by Kurucz et al. (1984) for the different enhancement factors of the van der Waals broadening ($E = 1$ and 2) (Fullerton & Cowley 1971) and their resulting abundances in comparison to the reference abundances by Bensby et al. (2014). We also show the theoretical spectral line that reproduces the equivalent width for the fixed abundance of Bensby et al. (2014) to illustrate the influence of the adopted continuum level. We see that a similar continuum treatment for the case of the Cr I line returns the reference abundance for $E = 2$ and an abundance that is 0.1 dex higher for $E = 1$. The different continuum level for the Mg I line provides 0.2 dex higher abundance even in the case of $E = 2$. We should not underestimate the importance of these factors when attempting to compare with results by other authors.

For the solar lines, this gave us a larger error than for the same elements in the stellar spectra (Fig. 9). However, the systematically lower $\log g$ that we found for our stars in common (Fig. 8) using the line data by Bensby et al. (2014) comes from the overabundance of Fe II lines due to the same reasons discussed above.

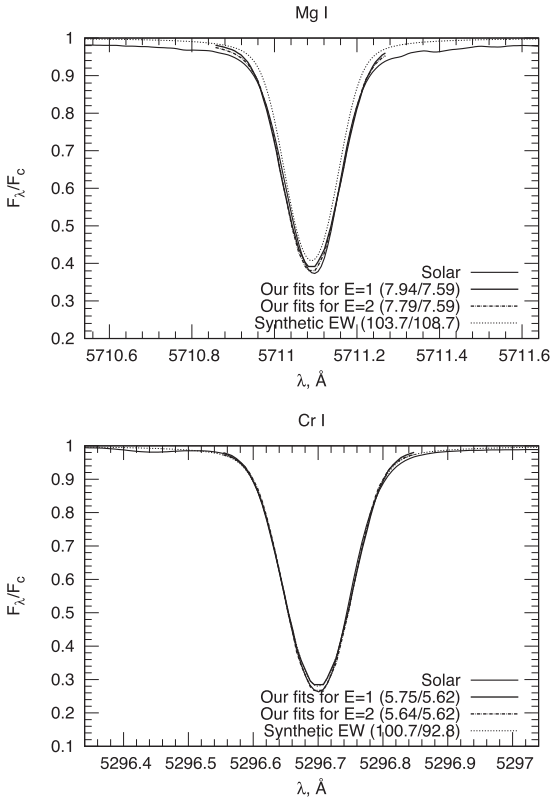

Figure 10. Fits for the different correction factors of the van der Waals broadening ($E = 1$ and 2). The numbers in brackets stand for the resulting abundance of the fit (left-hand panel) and the reference abundance by Bensby et al. (2014) (right-hand panel). 'Synthetic EW' is the theoretical spectral line for the fixed reference abundance by Bensby et al. (2014). The numbers in brackets depict the equivalent width of the theoretical line and the reference equivalent width measured by Bensby et al. (2014), respectively. 'Solar' is the observed solar spectrum by Kurucz et al. (1984) with their standard continuum level.

6 DISCUSSION

6.1 Results and comparisons

Our CHEPS sample is quite diverse in terms of surface gravity and effective temperature, and yet it maintains homogeneity in various senses. For instance, the selected stars generally have low chromospheric activity, meaning that the spectra of our sample should be minimally affected by spotty activity caused by magnetic field phenomena. Also, all of our stars are from the nearby solar neighbourhood, the distance does not exceed 170 pc and most of them belong to the thin disc population (Fig. 1).

Over the last few years, a few extended studies of the atmospheric abundances of stars with F–G spectral classes have been performed using various approaches. It is worth noting that in our analysis we used a different procedure in comparison to other authors. The use of line profiles allows us to develop an advanced procedure of the abundance analysis:

(i) We determined the distribution of microturbulent velocities in the atmospheres of our stars using the known condition $D_a = 0$; the distribution of V_m found in Fig. 5 covers the range of 0.8–1.4 km s^{-1}, with a maximum at 1.2 km s^{-1}.

(ii) To minimize the effects of blending, we used only parts of the absorption line profiles that are less affected by other lines. The use of our procedure is better suited to the case of metal-rich stars due to the increased line blending effects.

(iii) Our analysis allowed us to determine rotational velocities (Fig. 3). Furthermore, we showed that our fast-rotating stars have lower $\log g$, as expected for a population of younger stars.

(iv) We used only the effective photometric temperatures from Jenkins et al. (2008) as an input parameter to provide the complete analysis of our stellar spectra. The other parameters, i.e. [Fe/H], $V_r \sin i$, V_m and $\log g$, were found iteratively from the fits to observed absorption line profiles in the spectra.

In the framework of this work, we performed a direct comparison between our results and those of the other authors. We find the following:

(1) The abundance distributions of the metal-rich samples of stars from our work and those of the other authors are shown in Fig. 4. We see notable differences between all of the different samples, and hence we neglect analysing the mean sample abundances, giving preference to the trends of abundances with metallicities, since they are generally the same for the different authors.

(2) In Fig. 5, we show the microturbulent velocity distributions of our sample and the samples of the other authors. The adopted or determined microturbulent velocity is of crucial importance for the determination of accurate chemical abundances (Fig. 2). We can see that our distribution of V_m is narrower in comparison to the samples of Sousa et al. (2011), Adibekyan et al. (2012) and Bensby et al. (2014). A notable fraction of their stars show lower V_m, which formally should convert into larger measured abundances. In some sense, the shape of the V_m distribution reflects some of the uncertainties in the procedures of abundance determination: fits to the 'true' continuum, line blending, differences in *gf*, etc. Basically, we would expect a rather narrow distribution of V_m, due to the fact that the convective envelopes of solar-like stars on the main sequence, and those just moving off on to the subgiant branch, should be very similar.

(3) The abundance distributions of common elements for the samples of different authors are shown in Fig. 4. We can see here that the internal agreement is better than the absolute agreement. In

Table 2. The solar abundance analyses using our line list based on VALD-2 and VALD-3, and using the line list by Bensby et al. (2014) in comparison to the abundances determined by Bensby et al. (2014). The reference solar scales by Anders & Grevesse (1989) and Asplund et al. (2009) are shown in the last two columns.

	VALD-2	VALD-3	Bensby list	Bensby results	AG89	AS09
$\log g$	4.47	4.64	4.34	4.42	–	–
$V_{\rm m}$	1.0	1.0	1.0	0.88	–	–
$V_r \sin i$	1.73 ± 0.12	1.65 ± 0.11	1.84 ± 0.12	–	–	–
Na I	-5.72 ± 0.03	-5.76 ± 0.02	-5.54 ± 0.15	-5.81 ± 0.00	-5.71 ± 0.03	-5.80 ± 0.04
Mg I	-4.29 ± 0.09	-4.41 ± 0.16	-4.30	-4.45 ± 0.01	-4.46 ± 0.05	-4.44 ± 0.04
Al I	-5.58	-5.55	-5.51	-5.59 ± 0.00	-5.57 ± 0.07	-5.59 ± 0.03
Si I	-4.51 ± 0.11	-4.33 ± 0.02	-4.51 ± 0.02	-4.54 ± 0.01	-4.49 ± 0.05	-4.53 ± 0.03
Ca I	-5.64 ± 0.03	-5.71 ± 0.01	-5.72 ± 0.08	-5.71 ± 0.01	-5.68 ± 0.02	-5.70 ± 0.04
Ti I	-7.01 ± 0.04	-7.10 ± 0.03	-7.10 ± 0.03	-7.14 ± 0.08	-7.05 ± 0.02	-7.09 ± 0.05
Ti II	-6.98 ± 0.21	-7.09 ± 0.16	-7.14 ± 0.08	-7.14 ± 0.10	–	–
Cr I	-6.35 ± 0.03	-6.44 ± 0.02	-6.22 ± 0.06	-6.41 ± 0.01	-6.37 ± 0.03	-6.40 ± 0.04
Fe I	-4.42 ± 0.03	-4.43 ± 0.03	-4.46 ± 0.02	-4.49 ± 0.07	-4.37 ± 0.03	-4.54 ± 0.04
Fe II	-4.46 ± 0.02	-4.47 ± 0.04	-4.47 ± 0.02	-4.48 ± 0.08	–	–
Ni I	-5.73 ± 0.03	-5.77 ± 0.03	-5.77 ± 0.02	-5.81 ± 0.03	-5.79 ± 0.04	-5.82 ± 0.04

other words, comparing relative results between stars using a given methodology is more robust than comparing absolute results from different procedures directly. On the other hand, different authors also generally use different samples; therefore, hypothetically, absolute differences can be explained by differences in the local abundance distributions in the Galaxy, particularly, when comparing small numbers of stars. The comparison of common stars (Fig. 7) partially proves this, as we see a little bit better agreement for them, even despite the differences in the adopted input parameters, i.e. $T_{\rm eff}$, $\log g$ and $V_{\rm m}$, except for a few elements with a limited number of 'good' lines. However, we reiterate that it is still likely that we are seeing here the effects of the differences in the procedures adopted by each author, like the use of different line lists, adjusting parameters, quality of spectra, different interpretations of line blending effects, as well as systematic errors in the effective temperatures and/or gravities.

(4) Modern procedures aim to analyse huge sets of spectral data using automated routines or manually (e.g. Valenti & Fischer 2005; Adibekyan et al. 2012; Bensby et al. 2014; Brewer et al. 2016; Soto & Jenkins 2017). In our analysis, we also used the comparatively old classical results by Edvardsson et al. (1993) and Feltzing & Gustafsson (1998) that were carried out in the framework of the classical approach. In Fig. 4, we show only a few of the known abundance distributions obtained by different authors using different procedures. Santos, Israelian & Mayor (2004), Sousa et al. (2008, 2011), Neves et al. (2009) with Adibekyan et al. (2012), and Valenti & Fischer (2005) with Brewer et al. (2016), obtained extended abundance determination sets in the framework of the same procedures (the type of analysis, model atmospheres, line lists selection and the spectra). As expected, their results agree well, and therefore the similarities between these works are yet another reason to use independent procedures, like the one we used in our paper, for verification purposes. Various approaches provide notable differences between authors that exceed the internal accuracy of each method, e.g. Valenti & Fischer (2005) with Brewer et al. (2016) and Bensby et al. (2014) with Battistini & Bensby (2015).

(5) We obtained notable differences at the level of 0.2 dex for Mn abundances in the atmospheres of metal-rich stars between our work and those computed by Battistini & Bensby (2015) and Adibekyan et al. (2012). In most cases, this level of offset could be explained by differences in the adopted line lists. On the other hand, slopes of the dependence between [Mn/Fe] and [Fe/H] agree well between all comparison works (Table A1). It is interesting to note that Feltzing & Gustafsson (1998) and Brewer et al. (2016) obtained very similar results for this element (Fig. 4).

(6) Despite the different mean abundances in the samples, all comparison works show mostly the same trends with metallicity. Even if the computed numbers might be different (Table A1), the distributions in Fig. 4 point to the fact that differences in numbers might originate from the sample bias and border effects, as well as from a relatively large spread of abundances for certain elements like Mg, Al, Ti, Mn and Zn. Despite these differences, general trends remain the same.

(7) Only 12 stars from our sample have the confirmed planetary systems to date (see Jenkins et al. 2013b, 2017). Similarly to the other studies, for example, Valenti & Fischer (2005) and Neves et al. (2009), we found that the abundance distributions for hosts and stars without planets show no significant differences in the solar and metal-rich domains. Adibekyan et al. (2012) found the overabundance of α-elements for planet-hosting stars at low metallicities, though since we have only metal-rich stars, we cannot verify this result.

6.2 Differences between the samples

We can suggest a few possible explanations of the apparent differences in Fig. 4 between different authors:

(1) Astrophysics: Different samples draw stars that reach us from different parts of the Galaxy. We understand stellar nucleosynthesis, whereby metal-rich stars that were formed at distances of a few kpc from the Sun were formed in the epoch after the birth of the Sun. However, most of our stars belong to the thin disc that is well mixed due to the high stellar density. Eventually, we hope to measure all the abundances for stars near the Sun, such that we can say something more definite about the homogeneity of the local population.

(2) Differences in the details of procedures: To get matched abundances, it is necessary to perform fits to observed spectra, i.e. line profiles or equivalent widths, using the same procedures as those that were used in the literature. Three main sets of input data should be used: observed spectra, model atmospheres and line lists.

Overall, we can describe the differences in the abundance distribution of an element $\Delta_{\rm total}$ by the formula

$$\Delta_{\rm total} = \Delta_{\rm ma} + \Delta_{\rm Teff}^{\rm logg} + \Delta_{gf} + \Delta_X,$$

where

(i) $\Delta_{\rm ma}$ is the difference due to model atmosphere structures computed by different authors. We do not expect large differences here. Our experience shows that in most cases $\Delta_{\rm ma} < 0.1$ dex. Indeed, well-known programs that employ 1D model atmosphere computations, for example, ATLAS, MARCS, NEXTGEN, SAM12, use practically the same equation of state, opacity sources and convection treatments. Some differences here may be caused by abundance peculiarities, but it is not the case for solar-like dwarfs.

(ii) $\Delta_{\rm Teff}^{\rm logg}$ is the difference between the adopted or computed $T_{\rm eff}$ and $\log g$ converted into abundances. The determination of effective temperatures for stars remains a problem for these kinds of investigations. Different methods of $T_{\rm eff}$ determination could be characterized as photometric, spectroscopic and bolometric. Unfortunately, only the last one has a simple physical meaning. The spectroscopic $T_{\rm eff}$ really corresponds to the temperatures in line-forming regions of model atmospheres, i.e. above the photosphere layers where the main source of energy originates. In our work, we used photometric $T_{\rm eff}$, which is more similar to bolometric $T_{\rm eff}$. Differences between the $T_{\rm eff}$ of the star may be of the order of 50–100 K, which translates into abundance differences up to 0.2 dex for neutral iron.

(iii) Δ_{gf} represents the difference caused by uncertainties in the atomic line data for the absorption lines. There are no conventional line lists selected and approved for this kind of work, and every group uses their own pre-selected list of 'good' lines. Moreover, often oscillator strengths of some lines are adjusted for the best fits to solar spectrum. The cumulative effect of these updates can be seen in Fig. 4. As we noted above, the internal agreement of the results is better than the agreement between the different authors. The effects of solely oscillator strengths and different adoption of the same line list can be seen on the solar spectrum analysis in Table 2: We found that even VALD-2 and VALD-3 provide notable differences in the spectroscopic parameters of the same lines of some elements. The damping constants treated differently also provide the abundance differences up to 0.2 dex.

There is also a contribution to the Δ_{gf} due to a particular choice of the solar abundances at the line-pre-selection stage. It can result in the different mean abundances shown by different authors, too. Our comparison works relied mostly on the scales by Anders & Grevesse (1989) (most of the works shown in Fig. 4), Asplund et al. (2009) (oscillator strengths in Bensby et al. 2014) and their derivatives. These scales are not that much different in terms of the abundances, except Fe. What is more important is that our main selection criteria for our line list were a good fit to the observed solar line profiles – we did not aim to specifically describe our reference scale. Therefore, our resulting solar abundances are more clearly defined by the atomic line data we took from VALD than by the reference scale (Table 2).

(iv) Δ_X represents the possible detrimental effects caused by all other factors. For example, usually authors use pre-selected line lists that have been drawn from the analysis of a solar spectrum. To be certain in the line list output, it is important to adopt the similar continuum level. The ideal way would be to process the solar spectra using the same pipeline procedures as those used for the stars in the sample. This will enhance the determination accuracy of the stellar fundamental properties in relation to the Sun.

Although this is sensible, we should still account for the fact that blending effects increase in the spectra of metal-rich stars, or stars that rotate faster, which is one of the principal reasons why we used synthetic spectrum fits to observed spectra to determine our abundances. Finally, we should also note a few other possible effects that can contribute to the Δ_X parameter. For instance, non-LTE effects should be fully considered, and more sophisticated models of microturbulent and macroturbulent velocities, stellar variability and different kinds of stellar activity can also contribute.

7 SUMMARY

We carried out a spectral analysis of 107 metal-rich ([Fe/H] $\geq$ 7.67 dex) target stars from the CHEPS programme observed with HARPS to determine the abundances of Na, Mg, Al, Si, Ca, Ti, Cr, Mn, Fe, Ni, Cu and Zn in their atmospheres. We used the independent procedure of finding the best fit to the absorption line profiles in high-resolution spectra. The abundances, rotational velocities, microturbulence velocities and surface gravities were found using this iterative process.

Our analysis allowed us to determine the positively skewed normal distribution of projected rotational velocities with a maximum peaking at 3 km s^{-1}. We obtained a Gaussian distribution of microturbulent velocities that has a maximum at 1.2 km s^{-1} and a full width at half-maximum $\Delta v_{1/2} = 0.35$ km s^{-1}, indicating that metal-rich dwarfs and subgiants in our sample have a very restricted range in microturbulent velocities in comparison to samples of other authors, and independent of the number of stars. We also confirm that the abundance distributions for planet hosts and stars without planets show no significant differences, at least for our sample.

For most of the elements, our abundances agree up to $\pm$0.05 dex or better for the stars in common with other works. However, we do find systematic differences between the mean abundances in general samples. Our analysis suggests that the selection of line lists and atomic line data along with the adopted continuum level influences these differences the most.

The observed trends with metallicity remain as a reliable marker for the study of the chemical evolution of the Galaxy, as they remain the same across all comparison works despite differences in the spectra, methods and input data. We confirm the positive trends of abundances versus metallicity for Na, Mn, Ni, Zn and, to a lesser degree, Al. A slight negative trend is observed for Ca, whereas Si and Cr tend to follow iron.

ACKNOWLEDGEMENTS

We acknowledge funding by the EU FP7 Marie Curie Initial Training Networks (ITN) RoPACS project (GA N 213646) and the special support by the National Academy of Sciences (NAS) of Ukraine under the Main Astronomical Observatory GRAPE/GPU/GRID computing cluster project. We also acknowledge funding by BASAL Center for Astrophysics and Associated Technologies (CATA-Basal) grant (PB06, Conicyt), from Fondecyt through grants 1161218 and 3110004, partial support from Centro de Astrofísica FONDAP 15010003, the GEMINI-CONICYT FUND and from the Comité Mixto ESO-GOBIERNO DE CHILE and support from the UK Science and Technology Facilities Council (STFC) via grants ST/M001008/1 and Leverhulme Trust RPG-2014-281. This publication makes use of data products from the Two Micron All Sky Survey, which is a joint project of the University of Massachusetts and the Infrared Processing and Analysis Center/California Institute of Technology, funded by the National Aeronautics and

Space Administration and the National Science Foundation; ESA, 1997, The Hipparcos and Tycho Catalogues, ESA SP-1200; The VALD database, operated at Uppsala University, the Institute of Astronomy RAS in Moscow, and the University of Vienna; And the SIMBAD data base operated at CDS, Strasbourg, France (Wenger et al. 2000). We thank the anonymous referee for her/his thorough review and highly appreciate the comments and suggestions, which significantly contributed to improving the quality of the publication.

REFERENCES

Adibekyan V. Zh., Sousa S. G., Santos N. C., Delgado M. E., Gonzalez H. J. I., Israelian G., Mayor M., Khachatryan G., 2012, A&A, 545, 32
Anders E., Grevesse N., 1989, Geochim. Cosmochim. Acta, 53, 197
Asplund M., Grevesse N., Sauval A. J., Scott P., 2009, ARA&A, 47, 481
Battistini C., Bensby T., 2015, A&A, 577, 18
Bensby T., Feltzing S., Oey M. S., 2014, A&A, 562, 71
Bond J. C. et al., 2008, ApJ, 682, 1234
Brewer J. M., Fischer D. A., Valenti J. A., Piskunov N., 2016, ApJS, 225, 2
Bruntt H. et al., 2002, A&A, 389, 345
Buchhave L. A. et al., 2012, Nature, 486, 375
Casagrande L., Ramírez I., Meléndez J., Bessell M., Asplund M., 2010, A&A, 512, 54
da Silva R., Milone A. de C., Rocha-Pinto H. J., 2015, A&A, 580, 18
Datson J., Flynn C., Portinari L., 2015, A&A, 574, 124
Delgado M. E. et al., 2015, A&A, 576, 69
Demarque P., Woo J., Kim Y., Yi S. K., 2004, ApJS, 155, 667
Edvardsson B., Andersen J., Gustafsson B., Lambert D. L., Nissen P. E., Tomkin J., 1993, A&A, 275, 101
Feltzing S., Gustafsson B., 1998, A&AS, 129, 237
Fuhrmann K., 2004, Astron. Nachr., 325, 3
Fullerton W., Cowley C. R., 1971, ApJ, 165, 643
Gillon M., Magain P., 2006, A&A, 448, 341
Gonzalez G., 1997, MNRAS, 285, 403
Gray D. F., 1976, The Observation and Analysis of Stellar Photospheres. Wiley-Interscience, New York
Holweger H., Heise C., Kock M., 1990, A&A, 232, 510
Ida S., Lin D. N. C., 2008, ApJ, 685, 584
Jenkins J. S., Jones H. R. A., Pavlenko Ya.V., Pinfield D. J., Barnes J. R., Lyubchik Yu., 2008, A&A, 485, 571
Jenkins J. S. et al., 2009, MNRAS, 398, 911
Jenkins J. S. et al., 2011, A&A, 531, 8
Jenkins J. S. et al., 2013, EPJ Web. Conf., 47, 05001
Jenkins J. S. et al., 2013, ApJ, 766, 67
Jenkins J. S. et al., 2017, MNRAS, 466, 443
Jofre E., Petrucci R., Saffe C., Saker L., de la Villarmois A. E., Chavero C., Gomez M., Mauas P. J. D., 2015, A&A, 574, 50
Kordopatis G. et al., 2013, ApJ, 146, 134
Kupka F., Piskunov N., Ryabchikova T. A., Stempels H. C., Weiss W. W., 1999, AAS, 138, 119
Kurucz R., Furenlid I., Brault J., Testerman L., 1984, Solar Flux Atlas from 296 to 1300 nm. National Solar Observatory, New Mexico
Livio M., Pringle J. E., 2003, MNRAS, 346, 42
Luck R. E., Heiter U., 2006, AJ, 131, 3069
Mann A.W., Brewer J.M., Gaidos E., Lépine S., Hilton E.J., ApJ, 145, 52
Mashonkina L., Gehren T., Shi J.-R., Korn A. J., Grupp F., 2011, A&A, 528, 87
Murgas F., Jenkins J. S., Rojo P., Jones H. R. A., Pinfield D. J., 2013, A&A, 552, 27
Neves V., Santos N. C., Sousa S. G., Correia A. C. M., Israelian G., 2009, A&A, 497, 563
Nissen P. E., 2015, A&A, 579, 15
Pavlenko Y. V., 1997, Ap&SS, 253, 43
Pavlenko Y. V., 2002, KPCB, 18, 32
Pavlenko Y. V., 2003, Astron. Rep., 47, 59
Pavlenko Y. V., 2017, KPCB, 33, 55
Pavlenko Y. V., Jenkins J. S., Jones H. R. A., Ivanyuk O. M., Pinfield D. J., 2012, MNRAS, 422, 542
Perryman M. A. C. et al., 1997, A&A, 323, 49
Piskunov N. E., Kupka F., Ryabchikova T. A., Weiss W. W., Jeffery C. S., 1995, A&AS, 112, 525
Prugniel Ph., Vauglin I., Koleva M., 2011, A&A, 531, 165, 25
Ryabchikova T., Piskunov N., Kurucz R. L., Stempels H. C., Heiter U., Pakhomov Yu., Barklem P., 2015, Phys. Scr., 90, 5
Santos N. C., Israelian G., Mayor M., 2004, A&A, 415, 1153
Santos N. C. et al., 2008, A&A, 487, 369
Santos N. C. et al., 2013, A&A, 556, 150
Shchukina N., Trujillo B. J., 2015, A&A, 579, 112
Shchukina N., Sukhorukov A., Trujillo B. J., 2016, A&A, 586, 145
Soto M. G., Jenkins J. S., 2017, MNRAS, in press
Sousa S. G., Santos N. C., Israelian G., Mayor M., Monteiro M. J. P. F. G., 2006, A&A, 458, 873
Sousa S. G. et al., 2008, A&A, 487, 373
Sousa S. G., Santos N. C., Israelian G., Mayor M., Udry S., 2011, A&A, 533, 141
Strutskie M. F. et al., 2006, AJ, 131, 1163
Tabernero H. M., Montes D., Hernandez J. I. G., 2012, A&A, 547, 13
Thoren P., Feltzing S., 2000, A&A, 363, 692
Tsantaki M., Sousa S. G., Adibekyan V.Zh., Santos N. C., Mortier A., Israelian G., 2013, A&A, 555A, 150
Unsold A., 1955, Physik der Sternatmospharen, MIT besonderer Berucksichtigung der Sonne. Springer-Verlag, Berlin
Valenti J. F., Fischer D. A., 2005, ApJS, 159, 141
Wenger et al., 2000, A&AS, 143, 9

SUPPORTING INFORMATION

Supplementary data are available at *MNRAS* online.

Table A2. The abundances and fundamental properties found for the stars in our sample.
Table A3. The fitting spectral ranges used in our work.

Please note: Oxford University Press is not responsible for the content or functionality of any supporting materials supplied by the authors. Any queries (other than missing material) should be directed to the corresponding author for the article.

APPENDIX: ADDITIONAL TABLES AND PLOTS

We provide here the table with the mean abundances and slopes found in this work and comparison works, and the tables with the abundances and fundamental properties for the stars in our sample and the spectral fitting ranges used in our work. We also include a full list of the common stars and their fundamental properties found by different authors. And, finally, we include the plots for the abundance dependences on $T_{\rm eff}$ and $\log g$. The latter are discussed in Section 4.4.

Table A1. The mean abundances [X/Fe] and their slopes ($X_f = \Delta$[X/Fe]$/\Delta$[Fe/H]) in this work, in Adibekyan et al. (2012) (A) and in Bensby et al. (2014) (B). Only the stars with [Fe/H] $\geq$ 7.67 dex were accounted. N_l is the total number of lines in the list, and $\rho(T_{\rm eff})$ and $\rho(\log g)$ are the Pearson product–moment correlation coefficients for [X/H] versus $T_{\rm eff}$ and $\log g$.

Element				Abundances and slopes					
	N_l	$\rho(T_{\rm eff})$	$\rho(\log g)$	[X/Fe]	[X/Fe]A	[X/Fe]B	X_f	X_fA	X_fB
Na I	9	−0.20	−0.14	0.10 ± 0.08	0.09 ± 0.11	0.07 ± 0.07	0.30 ± 0.07	0.28 ± 0.10	0.20 ± 0.06
Mg I	7	−0.43	−0.02	0.13 ± 0.05	0.01 ± 0.07	0.16 ± 0.07	0.10 ± 0.05	0.02 ± 0.07	−0.23 ± 0.06
Al I	8	−0.36	0.01	−0.03 ± 0.05	0.05 ± 0.12	0.15 ± 0.05	0.13 ± 0.05	0.01 ± 0.12	−0.01 ± 0.05
Si I	28	−0.43	−0.02	0.10 ± 0.05	0.02 ± 0.03	0.11 ± 0.04	−0.07 ± 0.05	0.06 ± 0.03	−0.04 ± 0.04
Ca I	23	−0.21	0.03	0.05 ± 0.05	−0.00 ± 0.04	0.09 ± 0.04	−0.15 ± 0.04	−0.26 ± 0.03	−0.14 ± 0.04
Ti I	23	−0.28	0.29	−0.01 ± 0.04	0.06 ± 0.08	0.06 ± 0.04	−0.03 ± 0.04	−0.22 ± 0.07	0.10 ± 0.04
Ti II	3	0.26	−0.08	−0.05 ± 0.08	0.02 ± 0.05	–	−0.21 ± 0.08	0.05 ± 0.05	–
Cr I	52	−0.20	0.11	0.03 ± 0.03	0.01 ± 0.02	0.10 ± 0.03	−0.07 ± 0.03	−0.05 ± 0.02	0.09 ± 0.03
Mn I	20	−0.46	0.16	0.25 ± 0.09	0.04 ± 0.06	–	0.53 ± 0.07	0.36 ± 0.05	–
Fe I	63	−0.28	0.08	–	–	–	–	–	–
Fe II	15	−0.29	0.15	0.00 ± 0.04	–	−0.00 ± 0.01	0.05 ± 0.04	–	0.01 ± 0.01
Ni I	25	−0.25	0.00	0.13 ± 0.03	0.02 ± 0.04	0.05 ± 0.04	0.13 ± 0.03	0.18 ± 0.03	0.22 ± 0.04
Cu I	9	−0.30	−0.01	0.02 ± 0.09	–	–	0.28 ± 0.08	–	–
Zn I	1	−0.56	0.11	0.29 ± 0.14	–	0.13 ± 0.11	0.29 ± 0.14	–	0.04 ± 0.11

Table A2. The abundances and fundamental properties found for the stars in our sample. Full version available online.

Name	Distance	$T_{\rm eff}$	Sp. $\log g$	Ph. $\log g$	Ph. [M/H]	$V_{\rm m}$	$V_r \sin i$	Fe I	...
HD 6790	105.93	6012	4.40	4.36	0.20	0.8 ± 0.2	4.7 ± 0.2	−0.06 ± 0.02	...
HD 7950	117.37	5426	3.94	3.83	0.17	1.2 ± 0.2	2.7 ± 0.1	0.11 ± 0.02	...
HD 8389	30.51	5243	4.52	4.46	0.40	1.2 ± 0.2	1.4 ± 0.1	0.32 ± 0.03	...
HD 8446	73.64	5819	4.14	4.15	0.28	1.2 ± 0.2	3.9 ± 0.1	0.13 ± 0.02	...
HD 9174	78.93	5577	4.05	4.03	0.10	1.2 ± 0.2	2.9 ± 0.1	0.26 ± 0.01	...
...	...	...	...	...	...	...	...	...	...

Table A3. The fitting spectral ranges used in our work. In the last column, we show the number of lines for that specific element in that range found in VALD-2, along with the lines of other elements. Full version available online.

Element	Fitting range	N_l
11.00	5148.790 – 5148.890	1
11.00	5682.540 – 5682.720	1
11.00	5688.110 – 5688.330	2
11.00	6154.140 – 6154.300	2
11.00	6160.650 – 6160.860	3
...	...	...

Table A4. Iron abundances in the atmospheres of common stars. The metallicity values are given in the solar scales adopted by the respective authors, and therefore cannot be compared directly. We also included the overlapping stars from the results of the automatic pipeline procedure by Kordopatis et al. (2013).

Name	$T_{\rm eff}$/log g/[Fe/H]	Reference	Name	$T_{\rm eff}$/log g/[Fe/H]	Reference
HD 8389	5378/4.50/0.47	Sousa et al. (2006)	HD 150936	5542/4.13/0.16	Jenkins et al. (2008)
	5283/4.37/0.34	Sousa et al. (2008)		5692/4.40/0.24	Bensby et al. (2014)
	5243/4.46/0.40	Jenkins et al. (2008)		5692/4.40/0.24	Battistini & Bensby (2015)
	5283/4.37/0.34	Adibekyan et al. (2012)		5542/4.12/-0.03	This paper
	5182/4.33/0.36	Tsantaki et al. (2013)			
	5222/4.44/0.45	Mann et al. (2013)	HD 152079	5785/4.38/0.32	Jenkins et al. (2008)
	5283/4.37/0.34	Delgado et al. (2015)		5726/4.35/0.16	Santos et al. (2013)
	5224/4.31/0.43	Brewer et al. (2016)		5785/4.38/0.29	This paper
	5243/4.52/0.32	This paper			
HD 13147	5502/3.99/0.16	Jenkins et al. (2008)	HD 154672	5655/4.15/0.21	Jenkins et al. (2008)
	5352/3.47/-0.17	Kordopatis et al. (2013)		5743/4.27/0.25	Santos et al. (2013)
	5502/3.94/0.03	This paper		5655/4.16/0.10	This paper
HD 23398	5592/4.09/0.44	Jenkins et al. (2008)	HD 165204	5557/4.35/0.30	Jenkins et al. (2008)
	5438/4.03/0.31	Kordopatis et al. (2013)		5637/4.37/0.28	Bensby et al. (2014)
	5592/4.10/0.38	This paper		5637/4.40/0.28	Battistini & Bensby (2015)
				5557/4.33/0.17	This paper
HD 38467	5721/4.18/0.22	Jenkins et al. (2008)	HD 170706	5698/4.17/0.24	Jenkins et al. (2008)
	5753/4.15/0.24	Brewer et al. (2016)		5718/4.31/0.22	Bensby et al. (2014)
	5721/4.18/0.10	This paper		5718/4.33/0.22	Battistini & Bensby (2015)
				5698/4.40/0.13	This paper
HD 40293	5549/4.33/0.13	Jenkins et al. (2008)	HD 185679	5681/4.34/0.14	Jenkins et al. (2008)
	5518/4.39/0.03	Kordopatis et al. (2013)		5724/4.08/0.12	Kordopatis et al. (2013)
	5549/4.51/0.00	This paper		5710/4.47/0.06	Bensby et al. (2014)
HD 42719	5809/3.96/0.24	Jenkins et al. (2008)		5710/4.50/0.06	Battistini & Bensby (2015)
	5962/4.36/0.23	Kordopatis et al. (2013)		5681/4.43/0.01	This paper
	5809/4.08/0.11	This paper			
HD 48265	5651/3.92/0.29	Jenkins et al. (2008)	HD 186194	5668/4.09/0.18	Jenkins et al. (2008)
	5798/3.95/0.36	Santos et al. (2013)		5713/4.16/0.20	Bensby et al. (2014)
	5789/4.09/0.38	Jofre et al. (2015)		5713/4.20/0.20	Battistini & Bensby (2015)
	5651/3.92/0.17	This paper		5668/4.30/0.07	This paper
HD 66653	5771/4.40/0.15	Jenkins et al. (2008)	HD 190125	5644/4.20/0.22	Jenkins et al. (2008)
	5809/4.42/0.09	Datson, Flynn & Portinari (2015)		5682/4.48/0.17	Bensby et al. (2014)
	5771/4.42/-0.05	This paper		5682/4.50/0.17	Battistini & Bensby (2015)
				5644/4.53/0.04	This paper
HD 77338	5290/4.90/0.22	Feltzing & Gustafsson (1998)	HD 193690	5558/4.58/0.24	Jenkins et al. (2008)
	5290/4.60/0.30	Thorén & Feltzing (2000)		5542/4.41/0.20	Brewer et al. (2016)
	5315/4.55/0.10	Jenkins et al. (2008)		5558/4.48/0.15	This paper
	5300/4.30/0.36	Prugniel, Vauglin & Koleva (2011)	HD 194490	5854/4.46/0.28	Jenkins et al. (2008)
	5440/4.36/0.28	Santos et al. (2013)		5857/4.33/0.08	Bensby et al. (2014)
	5315/4.42/0.16	This paper		5857/4.30/0.08	Battistini & Bensby (2015)
				5854/4.44/-0.04	This paper
HD 90520	5870/4.02/0.17	Jenkins et al. (2008)	HD 201757	5597/4.02/0.15	Jenkins et al. (2008)
	6008/4.16/0.25	Bensby et al. (2014)		5566/3.99/0.11	Kordopatis et al. (2013)
	6008/4.20/0.25	Battistini & Bensby (2015)		5597/4.23/0.05	This paper
	5870/4.08/0.06	This paper			
HD 107181	5581/4.01/0.26	Jenkins et al. (2008)	HD 218960	5732/4.24/0.21	Jenkins et al. (2008)
	5628/4.05/0.31	Brewer et al. (2016)		5796/4.09/0.20	Bensby et al. (2014)
	5581/4.17/0.22	This paper		5796/4.10/0.20	Battistini & Bensby (2015)
HD 126535	5284/4.61/0.13	Jenkins et al. (2008)		5732/4.27/0.05	This paper
	5305/4.46/0.07	Tabernero, Montes & Hernandez (2012)	HD 220981	5567/4.34/0.18	Jenkins et al. (2008)
	5284/4.65/0.10	This paper		5618/4.26/0.25	Bensby et al. (2014)
HD 143361	5505/4.44/0.06	Jenkins et al. (2008)		5618/4.30/0.25	Battistini & Bensby (2015)
	5503/4.36/0.22	Santos et al. (2013)		5567/4.33/0.11	This paper
	5505/4.42/0.18	This paper			

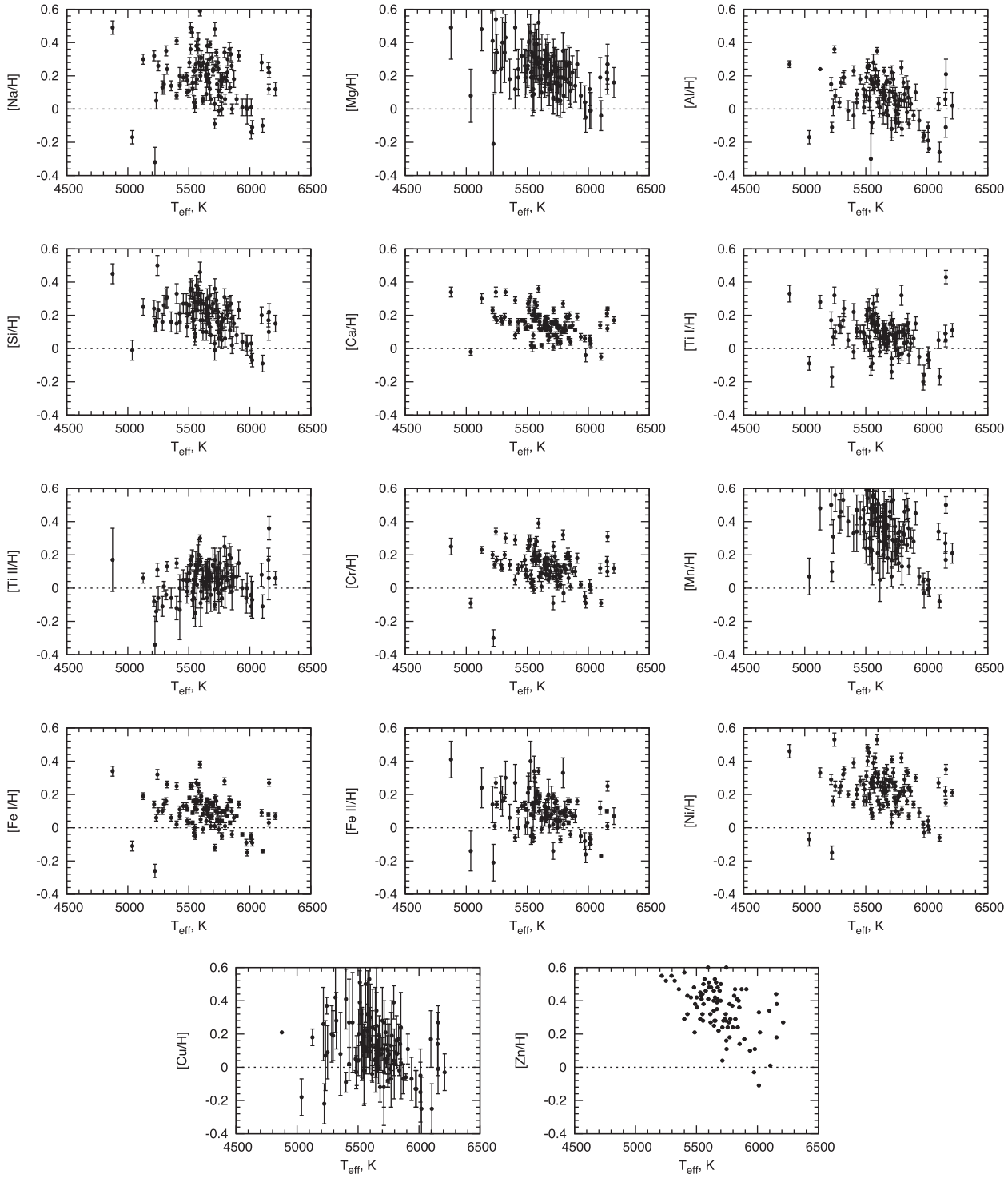

Figure A1. The dependences of [X/H] on $T_{\rm eff}$ in our sample.

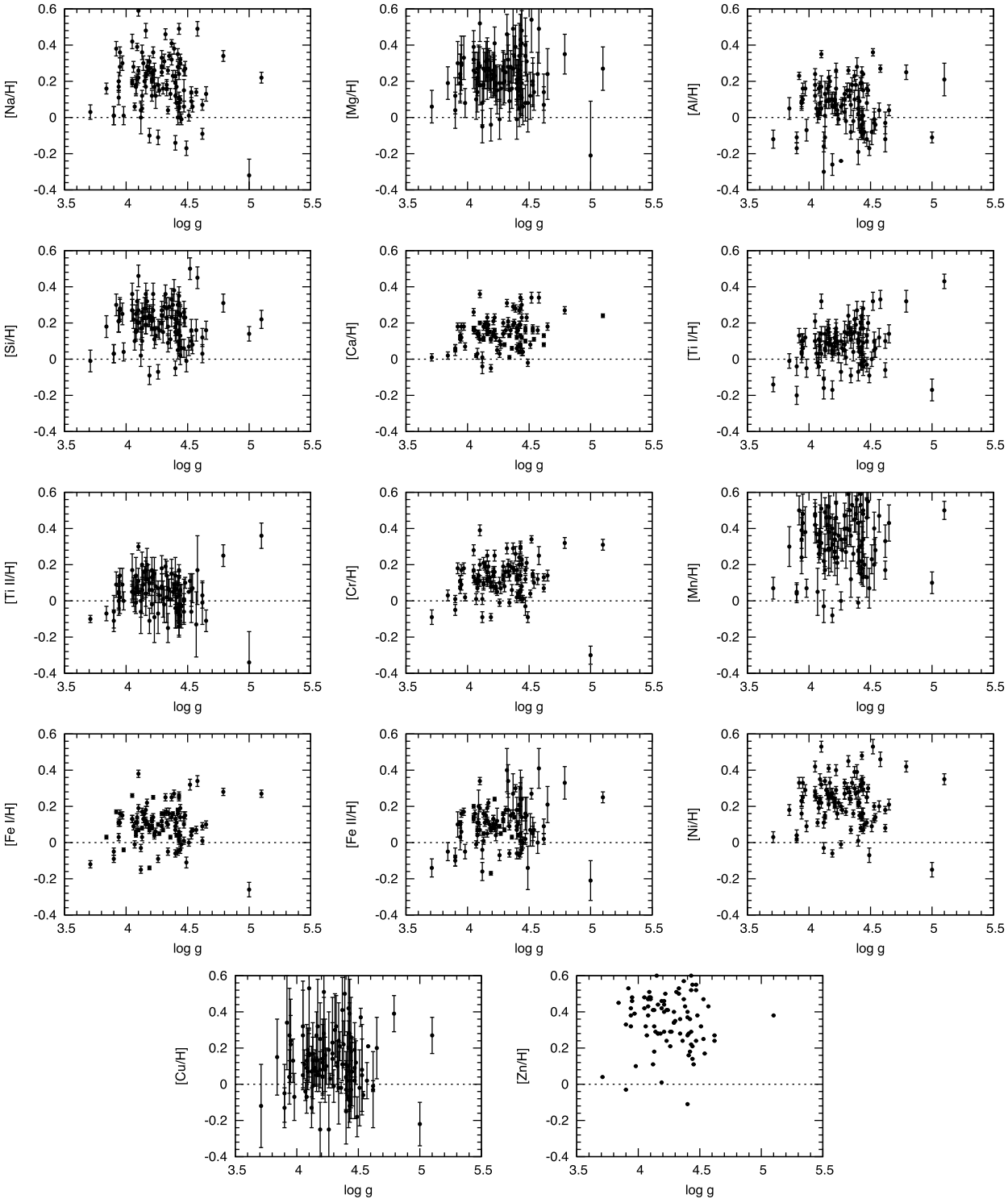

Figure A2. The dependences of [X/H] on log g in our sample.

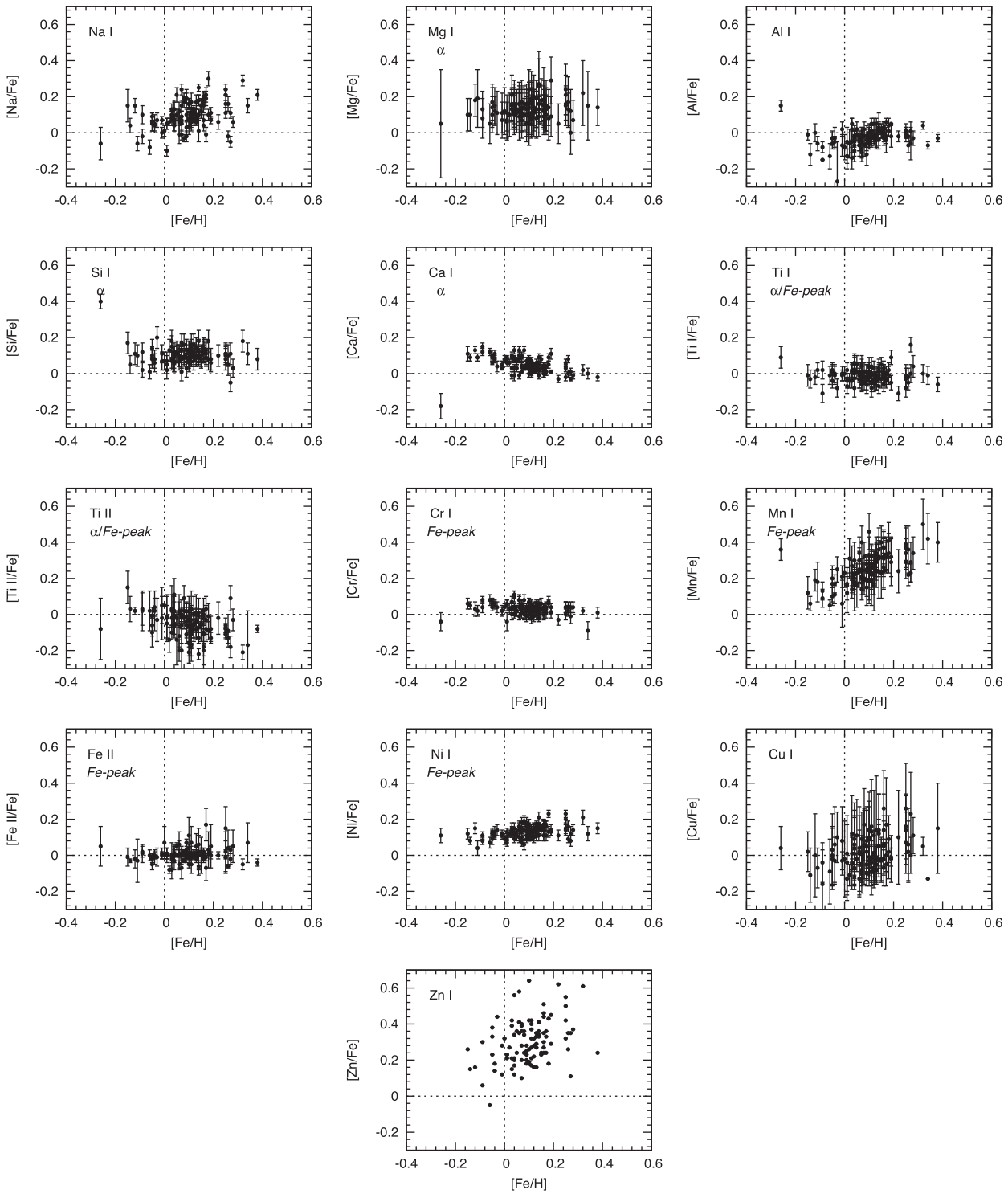

Figure A3. The dependences of [X/Fe] on [Fe/H] in our sample.

This paper has been typeset from a TEX/LATEX file prepared by the author.